

Lawrence Berkeley National Laboratory

Lawrence Berkeley National Laboratory

Title

Analysis of slice transverse emittance evolution in a photocathode RF gun

Permalink

<https://escholarship.org/uc/item/6bp1r5zj>

Author

Huang, Zhirong

Publication Date

2009-02-27

Analysis of slice transverse emittance evolution in a photocathode RF gun

Zhirong Huang, Yuantao Ding

Stanford Linear Accelerator Center, Stanford, CA 94309

Ji Qiang

Lawrence Berkeley National Laboratory, Berkeley, CA 94720 *

Abstract

The slice transverse emittance of an electron beam is of critical significance for an x-ray FEL. In a photocathode RF gun, the slice transverse emittance is not only determined by the emission process, but also influenced strongly by the nonlinear space charge effect. In this paper, we study the slice transverse emittance evolution in a photocathode RF gun using a simple model that includes effects of RF acceleration, focusing, and space charge force. The results are compared with IMPACT-T space charge simulations and may be used to understand the development of the slice emittance in an RF gun.

1. Introduction

Photocathode RF gun is one of the key enabling technologies for an x-ray free-electron laser (FEL). An important development in designing a photocathode RF gun is the emittance compensation [1], which is the process to align the transverse phase space of various temporal bunch slices under intense space charge in order to minimize the projected transverse emittance [2,3]. For a properly compensated electron beam, the projected transverse emittance is close to the emittances of individual temporal slices. Such a beam is easier to diagnose and to transport along the accelerator for producing FEL radiation.

Nevertheless, it is well-known that the x-ray FEL performance depends critically on the slice emittance (not the projected emittance), and the FEL interaction occurs much more rapidly on those slices with smaller emittances than others with larger emittances. Therefore, it is imperative to understand the slice emittance formation in a pho-

tocathode RF gun. Numerical simulations [4] show that the slice emittance growth (from its intrinsic or “thermal” level) can mainly be observed close to the cathode area, and has been attributed to the non-linear transverse space charge forces acting inside the bunch during the injection process. Motivated by these considerations, we develop a simple model to understand and quantify this emittance growth process. Using this model, we study the slice emittance evolution in a typical RF gun such as the one under commissioning at the LCLS [5].

2. Bunch Length Evolution

In order to model the transverse space charge effects near the cathode, we must first determine the bunch length evolution right after the bunch is born, where the electrons are still nonrelativistic and the bunch length is much shorter than the laser pulse length cT_L . As the bunch is accelerated in the RF gun, it elongates quickly into the final bunch length which is usually close to the laser pulse length. Tak-

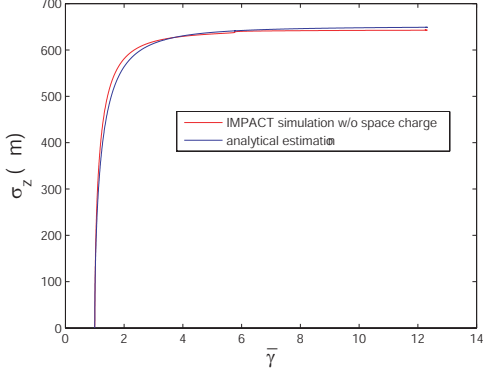


Fig. 1. IMPACT simulated rms bunch length without space charge and analytical estimation from Eq. (3). The flattop laser pulse length is $\Delta T_L = 10$ psec or 3 mm (rms $866 \mu\text{m}$).

ing into account the RF acceleration in the gun, a fitting formula that improve Kim's original model for the electron's final phase (relative to the RF, at $\gamma \gg 1$) is [6,7]

$$\phi_\infty = \phi_0 + \frac{1}{2\alpha \sin(\phi_0 + \pi/6\sqrt{\alpha})} + \frac{\pi}{15\alpha}. \quad (1)$$

Here ϕ_0 is the initial electron phase relative to the RF, $\alpha = eE_0/(2mc^2k)$, E_0 is the peak electric field, and k is the rf wavenumber (close to 60 m^{-1} for a S-band gun). The final bunch length in terms of the initial phase spread of the bunch is

$$kc\Delta T_f = \Delta\phi_\infty \approx \Delta\phi_0 \left[1 - \frac{1}{2\alpha} \frac{\cos(\phi_0 + \pi/6\sqrt{\alpha})}{\sin^2(\phi_0 + \pi/6\sqrt{\alpha})} \right]. \quad (2)$$

A typical RF gun runs at $\phi_0 = 30^\circ$ and compresses the final bunch length slightly compared to the laser pulse length (i.e., $\Delta T_f < \Delta T_L$).

To estimate the bunch length during the initial acceleration, we simply multiple ΔT_f by the average velocity $c\bar{\beta}$, i.e.,

$$L_b = \bar{\beta}c\Delta T_f = \sqrt{1 - \bar{\gamma}^{-2}} \frac{\Delta\phi_\infty}{k}. \quad (3)$$

where $\bar{\gamma}$ is the average beam energy in units of mc^2 . Figure 1 shows a numerical comparison of Eq. (3) to IMPACT-T simulation [8] in the absence of any space charge. Space charge effects at $\sim 1 \text{ nC}$ charges tend to lengthen the bunch and offset mild RF compression effect according to Eq. (1).

We will start our calculation assuming the bunch is just completely born at the cathode. The average energy is

$$\bar{\gamma}_0 \approx 1 + \frac{\bar{\beta}_0^2}{2}, \quad (4)$$

The initial average velocity can be estimated as follows. The head has velocity $(eE_0 \sin \phi_0/m)\Delta T_L$, and the tail has zero velocity, hence the average is

$$\bar{\beta}_0 = \frac{eE_0 \sin \phi_0}{2mc^2} c\Delta T_L. \quad (5)$$

3. Transverse Space Charge Modeling

After determining the bunch length and the charge density, we discuss the transverse space charge modeling. From Ref. [6], the transverse space charge of a cylinder bunch in the comoving beam frame is

$$E'_r(r, a) = \frac{\rho'}{4\pi\epsilon_0} 2a \int_0^\pi d\psi \cos \psi \log \left(\frac{R_- - s_-}{R_+ - s_+} \right), \quad (6)$$

where ρ' is the charge volume density in the beam frame, a is the radius of a uniform cross section, $r = \sqrt{x^2 + y^2}$ is the radial coordinate,

$$R_\pm = \sqrt{r^2 + a^2 - 2ra \cos \psi + s_\pm^2}, \quad (7)$$

$s_\pm = s \pm \frac{L'_b}{2}$, and $L'_b = \bar{\gamma}L_b$ is the beam frame bunch length.

Since the space charge fields vary slowly across the bunch, we focus our attention to the middle slice at $s = 0$ and drop the s dependence in the rest of the paper. Even when the initial laser transverse cross section is uniform, the self-consistent evolution of the transverse bunch distribution becomes quite complicated due to RF and space charge forces. Assuming cylindrical symmetry, the transverse space charge field for a circular ring shell from a to $a + da$ with a charge density $\rho'(a)$ is

$$E'_r(r, a + da) - E'_r(r, a). \quad (8)$$

The total transverse space charge can be found by adding contributions from all rings with the normalization

$$\int_0^{r_b} \rho'(a) 2\pi a da = \frac{Ne}{L'_b}, \quad (9)$$

where N is the total number of electrons, r_b is the maximum radius of beam cross section.

We can implement the above space charge field into a numerical code for an arbitrary transverse density distribution. Divide the total radial distance into $n(= 10)$ bins of equal (or unequal) radial separation $(0, r_1, \dots, r_n = r_b)$, count how many particles fall into each ring. If f_j is the fraction of particles in the j^{th} ring, then

$$\rho'_j = \frac{Ne}{L'_b} \frac{f_j}{\pi(r_j^2 - r_{j-1}^2)}. \quad (10)$$

and the transverse space charge field in the beam frame is

$$E'_r = \sum_{j=1}^n [E'_r(r, r_j) - E'_r(r, r_{j-1})]. \quad (11)$$

Transforming back to the lab frame, we have the space charge fields as

$$E_r^{SC} = \bar{\gamma} E'_r, \quad B_\theta^{SC} = \bar{\gamma} \frac{\bar{\beta}}{c} E'_r. \quad (12)$$

4. Paraxial Ray Equations

We use the paraxial expansion for both the RF and the solenoid fields. The RF fields are approximately given by

$$\begin{aligned} E_z^{RF}(r, z, t) &\approx \left[1 - \frac{r^2}{4} \left(\frac{\partial^2}{\partial z^2} - \frac{\partial^2}{c^2 \partial t^2} \right) \right] E_z(0, z, t), \\ E_r^{RF}(r, z, t) &\approx -\frac{r}{2} \frac{\partial E_z(0, z, t)}{\partial z}, \\ B_\theta^{RF}(r, z, t) &\approx \frac{r}{2c} \frac{\partial E_z(0, z, t)}{c \partial t}. \end{aligned} \quad (13)$$

where z is the longitudinal distance from the cathode. The solenoid field can be described as

$$\begin{aligned} B_z^{Sol}(r, z) &\approx \left(1 - \frac{r^2}{4} \frac{d^2}{dz^2} \right) B_z(0, z), \\ B_r^{Sol}(r, z) &\approx -\frac{r}{2} \frac{dB_z(0, z)}{dz}, \end{aligned} \quad (14)$$

Since both the RF and the solenoid fields possess cylindrical symmetry, the canonical angular momentum $p_\theta = \gamma m r^2 \dot{\theta} + e r A_\theta$ is a constant of motion ($A_\theta = r B_z(0, z)/2$ given by solenoid). The electron motion is governed by the Lorentz force as (see, e.g., Ref. [9], p.71)

$$\frac{d(\gamma m v_z)}{dt} = e E_z^{RF} + e v_r (B_\theta^{RF} + B_\theta^{SC}) - e v_\theta B_r^{Sol}, \quad (15)$$

$$\begin{aligned} \frac{d(\gamma m v_r)}{dt} &= e (E_r^{RF} + E_r^{SC}) - e v_z (B_\theta^{RF} + B_\theta^{SC}) \\ &\quad - \frac{m r}{4 \gamma} \left(\frac{e B_z^{Sol}}{m} \right)^2 + \frac{p_\theta^2}{\gamma m r^3}. \end{aligned} \quad (16)$$

Here $v_z = \dot{z}$, $v_r = \dot{r}$, $v_\theta = r \dot{\theta}$, $\gamma = (1 - v^2/c^2)^{-1/2}$, and $v^2 = v_r^2 + v_\theta^2 + v_z^2$ for each individual electron. We have ignored the longitudinal space charge force for these electrons that are assumed to be in the middle of the bunch. We have also found that including higher-order terms (than the second-order ones) in the paraxial field expansion do not change our numerical results shown in the next section.

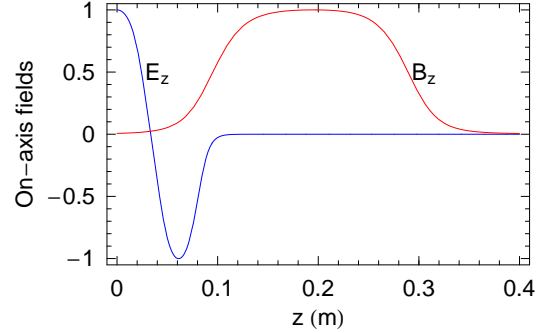


Fig. 2. The normalized on-axis RF and solenoid fields as functions of distance from cathode for the LCLS RF gun.

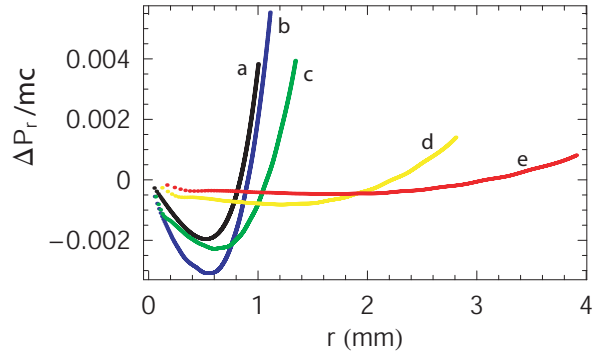


Fig. 3. Transverse momentum (after subtracting the linear correlation with r) as a function of the radial position r for the LCLS RF gun (1 nC charge, no solenoid) at various times: (a) $t=6.7$ ps (black), (b) $t=16.7$ ps (blue), (c) $t=33$ ps (green), (d) $t=167$ ps (yellow), and (e) $t=400$ ps (red).

For simplicity, we assume the electrons are born with zero canonical angular momentum (i.e., $p_\theta = 0$). This corresponds to the case when the solenoid magnetic field at the cathode is negligible or is canceled by the field from a bucking coil (i.e., $B(0, z=0) = 0$). In such a case, we can set $v_\theta = -e A_\theta / (\gamma m) = -e r B_z(0, z) / (2 \gamma m)$ in Eq. (15) and drop the last term in Eq. (16). Although electron's angular momentum $\gamma m r^2 \dot{\theta} = -e r A_\theta$ is not zero inside the solenoid, it vanishes once the electron leaves the solenoid field region. Thus, we only use $P_r = \gamma m v_r$ for the transverse momentum in computing the transverse emittance in this model as well as in the simulation studies.

5. Numerical Results and Discussions

In this section, we describe numerical solutions of the Lorentz equations (15) and (16) and compare

with the simulation results of the LCLS RF gun. The equations are solved in Mathematica. Typically, 400 macroparticles are launched at an initial RF phase corresponding to the center slice (e.g., $\phi_0 = 32^\circ$). The initial transverse distribution of these particles is assumed to be uniform in the cross section following a uniform illuminating laser spot (of radius 1 mm). The temporal profile of the laser is assumed to be flattop with a 10 ps pulse duration, and the electron bunch length evolution follows Eq. (3). The thermal emittance is taken to be zero (i.e., $P_r(t=0) = 0$) to illuminate the slice emittance growth mechanism. The on-axis RF and the solenoid fields are given externally and are shown in Fig. 2, with peak values $E_0 = 120$ MV/m and $B_0 = 2513$ G, respectively. We follow these particles in time. At a given time, we recalculate the space charge fields on a uniform radial grid based on the transverse distribution at that moment. Space charge fields at particle positions can be smoothly interpolated from these grid points.

Figure 3 shows a few snapshots of the transverse phase space ($r, \Delta P_r$) inside the RF gun in the absence of the solenoid, where ΔP_r is the residual transverse momentum after subtracting the linear correlation with r . The transverse phase space distortion occurs due to the nonlinear space charge near the cathode when the bunch is still non-relativistic and extremely short in length. The normalized rms emittance in the case of cylindrical symmetry can be calculated from

$$\epsilon_x^n = \epsilon_y^n = \frac{1}{2} \sqrt{\langle r^2 \rangle \langle P_r^2 \rangle - \langle r P_r \rangle^2}, \quad (17)$$

where $\langle \rangle$ means averaging over all particles. Figures 4 and 5 show comparison of the slice emittance and the rms beam size $\sigma_x = \sigma_y = \sqrt{\langle r^2 \rangle / 2}$ with IMPACT-T simulations for two bunch charges in the LCLS gun without solenoid focusing. The agreements are quite reasonable. The slice emittance grows rapidly within the first few mm from the cathode and then start to decrease. As indicated in Fig. 3, when the transverse beam size is increased due to space charge defocusing, the phase space distribution tends to become more linear. This self-linearizing process is also observed in numerical simulations of Ref. [4].

Figures 6 and 7 show the slice emittance and the rms beam size evolution at 1 nC charge with the focusing solenoid and a drift space (of about 1.1 m in length) following the solenoid before the booster linac. Although the simplified model shows a similarly complex behavior of the emittance evolution

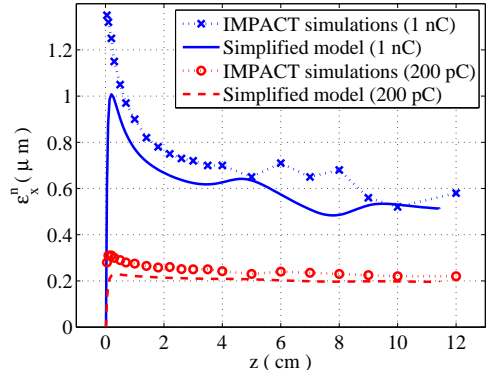


Fig. 4. Slice emittance evolution at 1 nC and 200 pC for the LCLS gun (no solenoid).

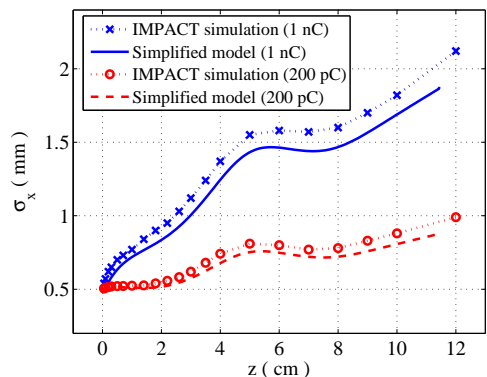


Fig. 5. RMS beam size evolution at 1 nC and 200 pC for the LCLS gun (no solenoid).

as the IMPACT-T simulation, there remains quantitative differences between the model and the simulation outside the solenoid region (beyond $z \approx 0.3$ m). The discrepancy in Fig. 6 might arise from the strong transverse focusing that causes the beam to converge after the solenoid. The convergence of the beam may couple different slices with each other through global space-charge forces which are not included in this simplified model. Further studies are necessary to understand this effect and to improve the model.

Acknowledgments

The authors would like to thank D. Dowell for discussions on beam formation near the cathode, C. Limborg for discussions on the LCLS injector simulations, and G. Stupakov for useful comments. This work was supported by the U.S. Department of Energy contracts No. DE-AC02-76SF00515.

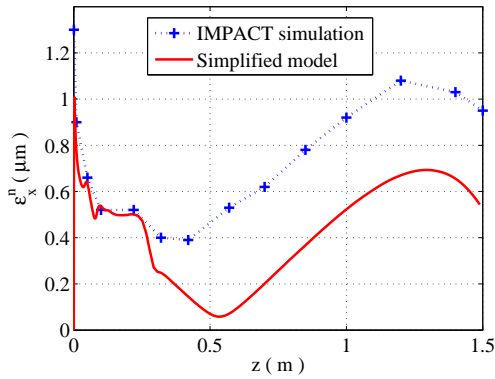


Fig. 6. Slice emittance evolution at 1 nC for the LCLS gun including the solenoid and the drift space before the booster linac.

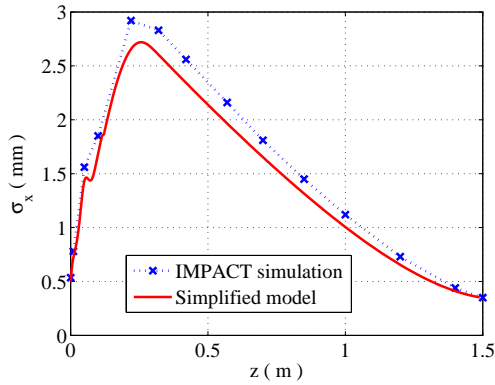


Fig. 7. RMS beam size evolution at 1 nC for the LCLS gun including the solenoid and the drift space before the booster linac.

References

- [1] B. Carlsten, Nucl. Instrum. Methods A **285**, 313 (1989).
- [2] L. Serafini and J. Rosenzweig, Phys. Rev. E **55**, 7565, (1997).
- [3] C.-X. Wang, Phys. Rev. E **74**, 046502, (2006).
- [4] R. Cee *et. al.*, Nucl. Instrum. Methods A **483**, 321 (2002).
- [5] D. Dowell *et. al.*, in Proceedings of 2007 Free-Electron Laser Conference, Novosibirsk, Russia, 2007.
- [6] K.-J. Kim, Nucl. Instrum. Methods A **275**, 201 (1989).
- [7] C. Travier, Nucl. Instrum. Methods A **340**, 26 (1994).
- [8] J. Qiang *et. al.*, Phys. Rev. ST Accel. Beams **9**, 044204 (2006).
- [9] M. Reiser, *Theory and Design of Charged Particle Beams*, John Wiley & Sons, Inc., New York, 1994.